Blunt cones in rarefied hypersonic flow: Experiments and Monte-Carlo simulations

G.A. Dahlen†, M.N. Macrossan‡, C.L. Brundin†, and J.K. Harvey‡*

June, 1984

† Department of Engineering Science, University of Oxford.
‡ Department of Aeronautics, Imperial College, London.

1 Introduction

The drag force that acts on the slender cone at zero angle of attack in a rarefied hypersonic flow has been measured for a range of bluntness ratios (R_n/R_b) and wall-to-stagnation temperature ratios (T_w/T_0). For some of the flows that have been studied experimentally, calculations have also been made using Bird's Direct Simulation Monte-Carlo method adapted to include the effects of internal energy exchange. Details of the flows and surface stresses are presented.

2 The experiment

The drag forces acting on cones with semi-vertex angle θ_c, equal to 3° and 6° have been measured in the Oxford University Low Density Wind Tunnel (ref. 1). This is equipped with a balance which magnetically suspends the model, thus eliminating errors due to sting interference. The working fluid, which is air, is expanded through an axisymmetric nozzle to a free-stream Mach number of between 5.2 and 5.9. A range of Knudsen numbers based on free-stream conditions of 0.006 to 0.05 was achieved by varying the stagnation pressure from 16 to 50 torr and by using two model sizes for each cone angle. The values of nose bluntness ratio tested were 0.0, 0.1, 0.2, 0.3 and 0.4 and the models had base diameters, D, of either 2.5mm, 5.0mm or 10.0mm. Each was constructed of either carbon steel. or fine-grain cast iron and ground with an r.m.s surface finish of better than 0.3μm. Cone angle and nose radius tolerances were 2′ and [12 m][1] respectively and the vertex truncation of the sharp cones was less than 0.25μm.

*Author's copy of: G. A. Dahlen, M. N. Macrossan, C. L. Brundin and J. K. Harvey, 'Blunt cones in rarefied hypersonic flow: experiments and Monte-Carlo simulations', *Proceedings of the* 14^{th} *International Symposium on Rarefied Gas Dynamics*, ed. H. Oguchi. University of Tokyo Press (1984), vol. I, pp. 229-240. ISBN 4-13-068109-5 (UTP 69092). Corresponding author's present address: M. N. Macrossan, Centre for Hypersonics, School of Engineering, University of Queensland, Australia 4072, m.macrossan@uq.edu.au

[1]Value now unknown. Perhaps 12μm. MNM July 2007

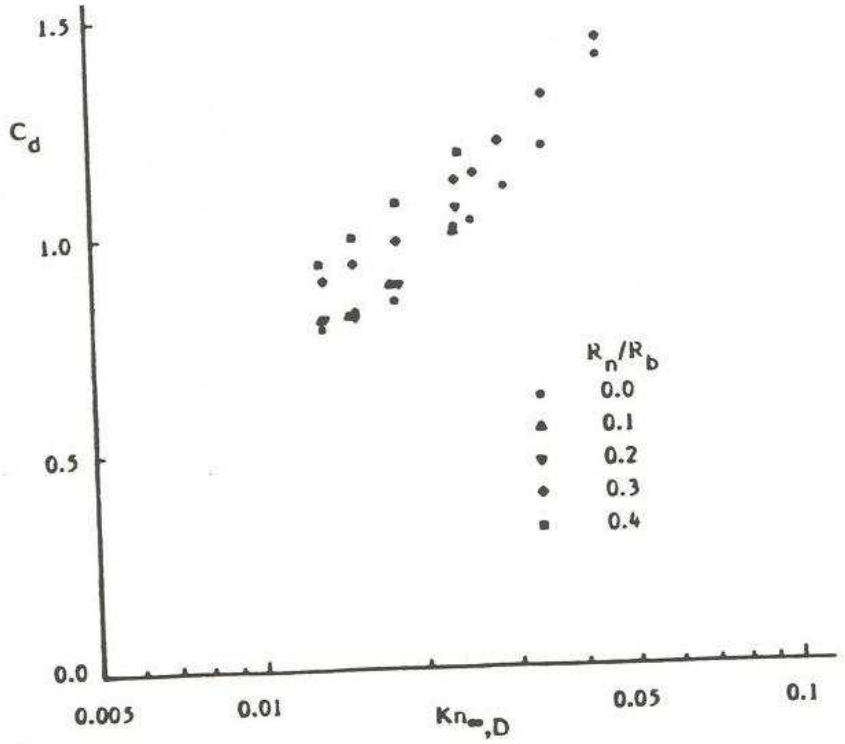

Figure 1: Nose bluntness effects on 3° cone drag ($T_w/T_0 = 1.0$).

Two nominal values of stagnation temperatures, 293K and 380K, were chosen. The temperature of the models, which could be pre-cooled in a separate chamber with liquid nitrogen, ranged from 293K down to 89K. The temperature at the moment at which the drag force was recorded was calculated by considering radiative and convective heat transfer. A rise of about 13K occurred between the time when the model was first suspended magnetically and when the reading was taken in the established test flow. Experimental errors in C_d are considered to be less than 2% and, in the determination of free-stream Knudsen number, less than 3%. The gradient of Mach number in the undisturbed test flow was no more than 1.7% for the longest model. Further details of the experimental procedures can be found in ref. 2.

3 Experimental results

Figs. 1 and 2 show the measured drag coefficients for cones with adiabatic walls and a range of bluntness ratios. The free-stream Knudsen number was calculated from

$$\mathrm{Kn}_{\infty,D} = 1.26\sqrt{\gamma}\frac{\mathrm{M}_\infty}{\mathrm{Re}_{\infty,D}}$$

where $\gamma = 1.4$. The viscosity at the low temperature experienced in the free-stream was calculated from the Chapman-Enskog integral evaluated for the Lennard-Jones (6-12) potential with a molecular size of $\sigma = 3.617$Å and a potential well depth of $T' = 97$K (ref. 3). For each test case the stagnation temperature was about 293K.

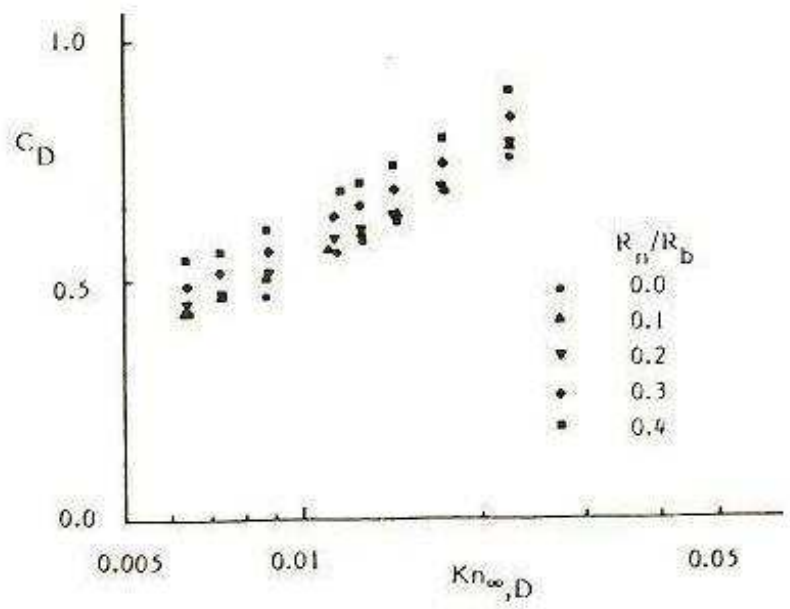

Figure 2: Nose bluntness effects on 6° cone drag ($T_w/T_0 = 1.0$).

All the results show that C_d rises with increasing bluntness. The effect is slight for $R_n/R_b < 0.2$ but a more pronounced uniform increase can be seen from $R_n/R_b = 0.2$ to 0.4. The results for the 6° cone show no indication that the drag coefficients for the sharp and blunt shapes converge at large Knudsen numbers. Contrastingly the measurements for the 3° cone appear to converge at around $\mathrm{Kn}_{\infty,D} = 0.5$.

The drag coefficient for the free molecular limit, $C_{d,fm}$ has been calculated for each body assuming diffuse reflections and complete thermal accommodation. For these free-stream conditions, this is found for the 6° cones to be greater for the blunt cases than for the sharp body. However the converse is true for the 3° cone. The convergence of the drag coefficients for the 3° and not for the 6° cones can thus be explained in terms of the free molecular limit behaviour. All of the measured results appear to be approaching this limit with increasing Knudsen number.

A study was made of the effect of reducing the wall-to-stagnation temperature ratio for the 6° cone with $R_n/R_b = 0.3$ and 0.4. The results taken at a higher stagnation temperature of about 380K, are presented in fig. 3 and show that in both cases C_d is reduced by only about 5% as the temperature ratio is changed from 0.78 to 0.23. Thus the influence of wall temperature on the drag mirrors very closely the free molecular behaviour where only the normal force is affected by T_w/T_0 and the dominant shear stress remains constant.

Attempts have been made to correlate the data for the range of R_n/R_b tested using Knudsen numbers based on a variety of characteristic lengths, for example, the square root of the wetted area or the length measured along the body from the apex to the base. Good correlations for each separate cone angle were achieved using normalised drag, $C_d/C_{d,fm}$ plotted against a free-stream Knudsen number based on the length of the cone, L. Data for the two vertex angles collapsed when L was replaced by $2L\tan\theta_c$ which is the base diameter in the case of the sharp cone. Fig. 4 shows all the data from figs. 1 to 3 and some additional results from ref. 2. The correlation works better for the 6° cone and there is still a slight separation of the 3° and 6° cone results.

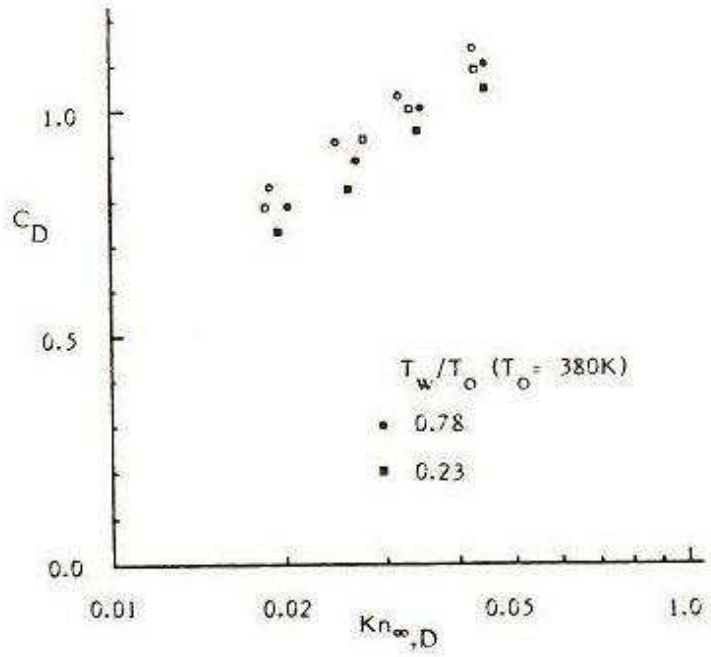

Figure 3: Wall temperature effect on blunt 6° cone drag. Open symbols, $R_n/R_b = 0.4$. Close symbols, $R_n/R_b = 0.3$.

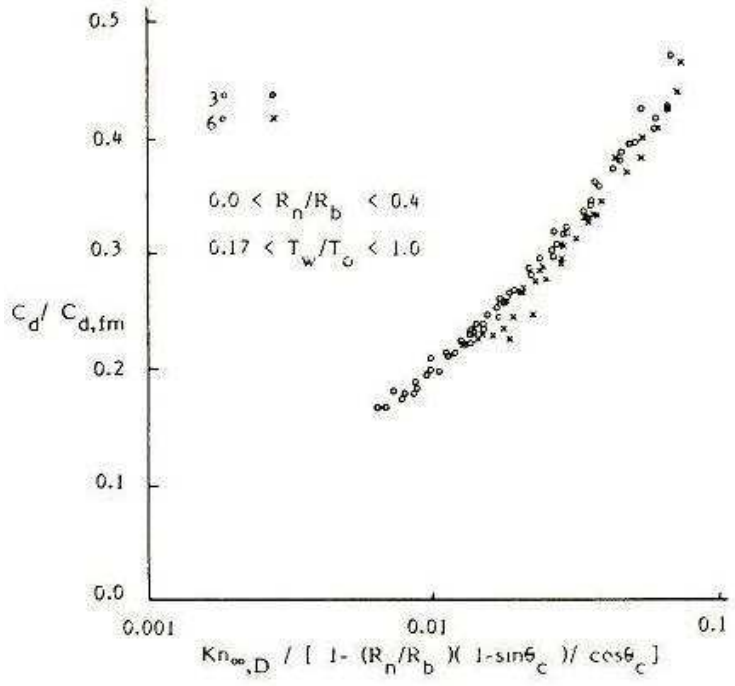

Figure 4: Correlation of blunt cone drag

4 Monte-Carlo Direct Simulation Calculations

The simulation calculations were made using a Morse potential variable-ϕ collision model (ref. 4). This potential, which incorporates long-range attractive intermolecular forces, gives a better representation of the viscosity at low temperatures than a purely repulsive potential. The variable-ϕ extension of Larsen and Borgnakke's phenomenological restricted exchange scheme (ref. 5) permits variations of the rotational relaxation rate with temperature.

The collision model was designed to match the properties of nitrogen as closely as possible. The results can, however, be compared with those obtained experimentally in air by adjusting the mean free path in the Knudsen number. The mean free path quoted for the Monte-Carlo results is

$$\frac{\Omega^{(2,2)*}\left(T_\infty/T'_N\right)}{\Omega^{(2,2)*}\left(T_\infty/T'_A\right)}\left|\frac{T'_A}{T'_N}\right|^{2/\alpha}\lambda_N$$

where λ_N is the value used in the calculation, $\alpha = 13.5$ and and T'_A and T'_N are the well depth temperatures for air and nitrogen, 97K and 91.5K respectively.

In all calculations it was assumed that molecules were diffusely scattered from the surface fully accommodated to the wall temperature.

5 Results of the Simulation Calculations

All the calculations were performed for a 6° cone with $R_n/R_b = 0.4$. The values of the drag coefficients are shown in fig. 5 and are in good agreement with the experimental results. They do not correlate as well as the experimental data which suggests that there is some statistical scatter in the computed values. The local pressure and shear stress coefficients for a range of densities are shown in fig. 6 for $T_w/T_0 = 1.0$ and in fig. 7 for $T_w/T_0 = 0.27$. The pressure shows significant statistical scatter but the shapes of both normal and shear stress envelopes are qualitatively similar down to $\mathrm{Kn}_{\infty,D} = 0.02$.

The drag coefficient can be separated into a contribution from the pressure $C_{d,p}$, and one from the shear $C_{d,s}$. Fig. 8 shows the division of the total drag into these two components. It is interesting to note that even at $\mathrm{Kn}_{\infty,D} = 0.02$ the shear accounts for 67% of the total drag compared with 83.3% in the free molecular limit. Fig. 9 shows the change in the pressure and shear drag as a fraction of their respective free molecular values for a range of Knudsen numbers and wall temperatures. The figure shows that as the flow becomes less rarefied the pressure drag remains closer to its free molecular value than does the shear. Thus the changes in drag due to reducing $\mathrm{Kn}_{\infty,D}$ are dominated by changes in the shear component. For diffuse reflections the theoretical value of the free molecular shear drag does not vary with wall temperature. This behaviour is echoed throughout the transitional regime examined here where the shear drag can be seen to be almost independent of T_w/T_0.

Figs. 10-12 shows density and rotational temperature contours for different wall temperatures. The rotational temperature has been chosen for presentation since this quantity is more easily measured than other temperature components. However, as the inset graph shows, rotational and translational temperatures stay in close equilibrium for all of the flow field except for the region close the body surface.

The density field shows a weak diffuse shock which is virtually unaffected by wall temperature. The temperature shows no sign of a discrete shock but it does overshoot the wall temperature for the coldest wall. The very diffuse compressive flows seen in this Knudsen

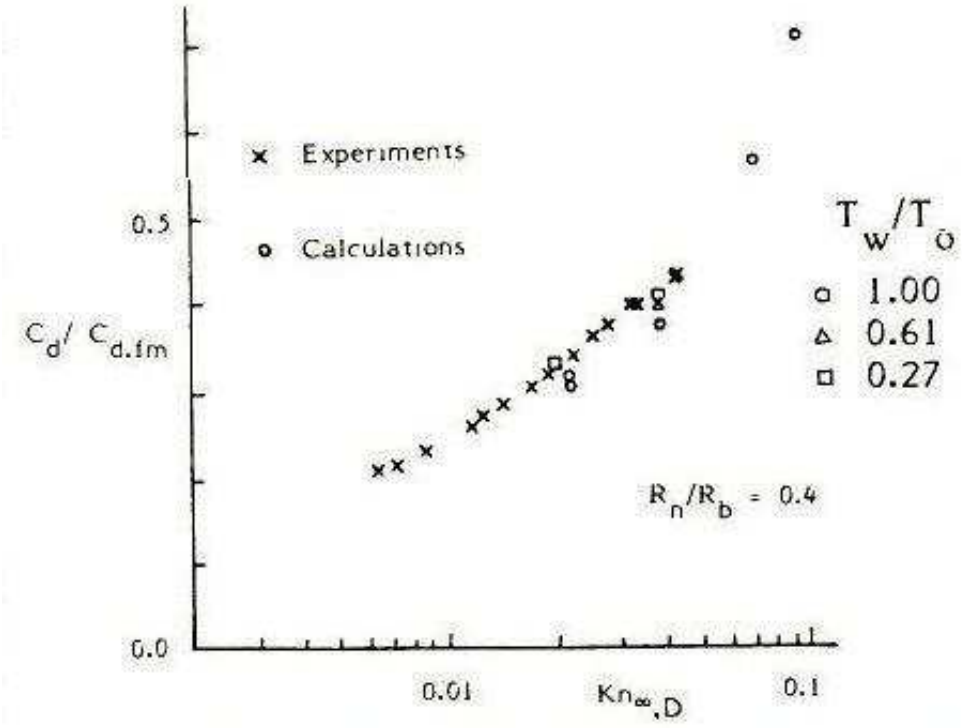

Figure 5: Monte-Carlo results compared with experiments

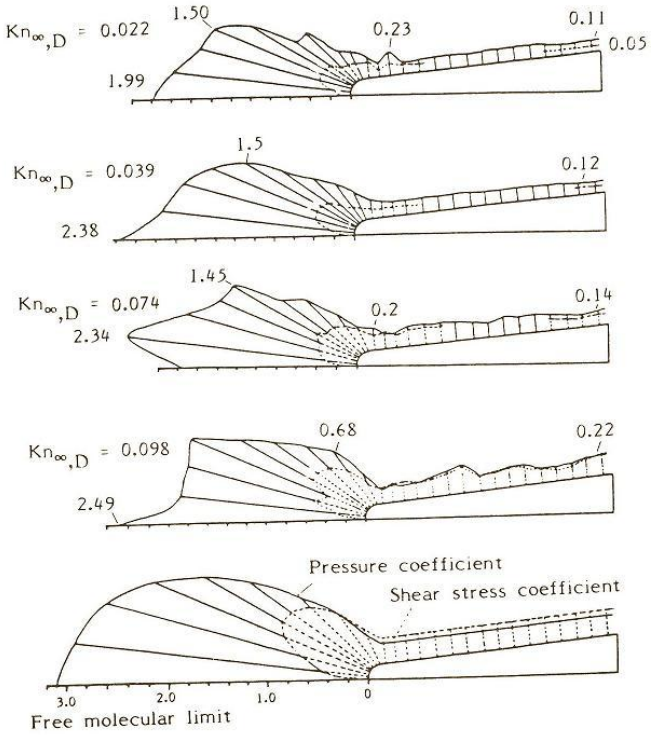

Figure 6: Distribution of pressure and shear stress coefficients ($T_w/T_0 = 1.0$). $\mathrm{Kn}_{\infty,D} = 0.022, 0.039, 0.074, 0.098, \infty$.

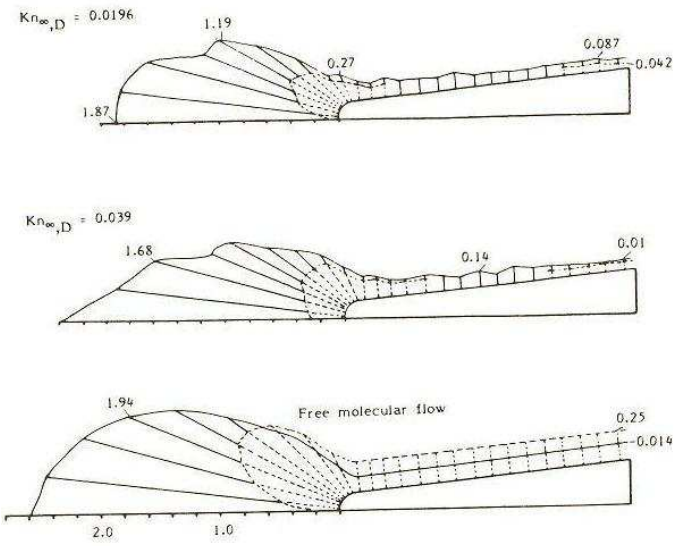

Figure 7: Distribution of pressure and shear stress coefficients ($T_w/T_0 = 0.273$). $\mathrm{Kn}_{\infty,D} = 0.0196, 0.039, \infty$.

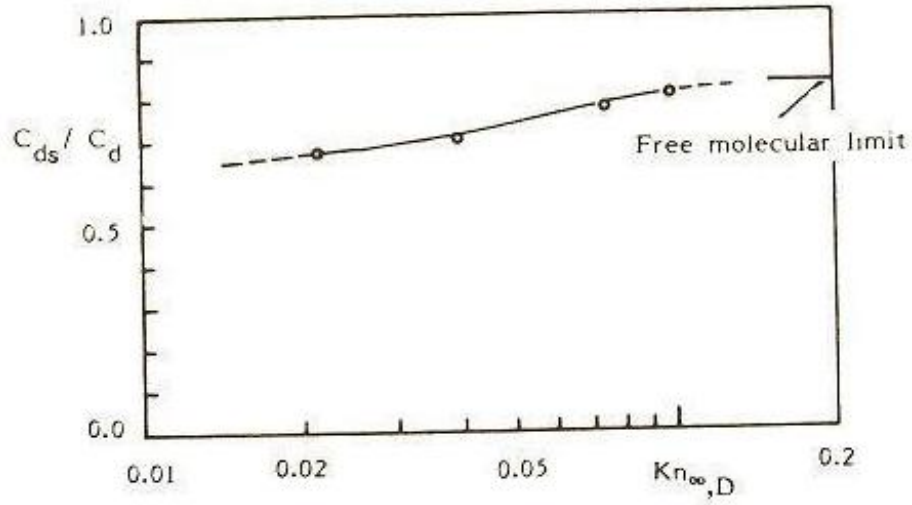

Figure 8: Shear drag as a fraction of the total computed drag.

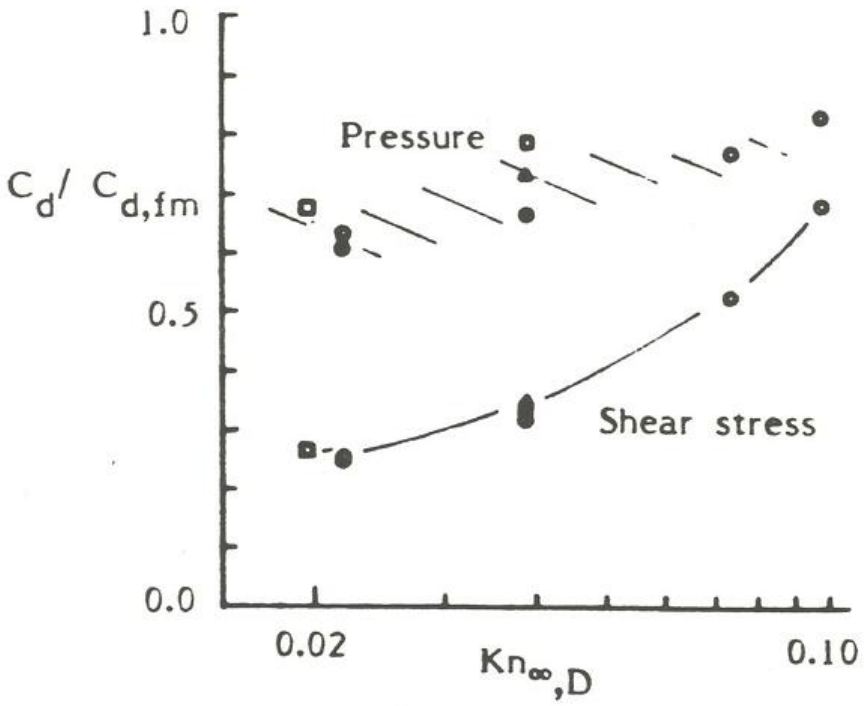

Figure 9: Variation of the pressure and shear drags with Knudsen number

number range show a much closer affinity to the free molecular limit than to that for a high Reynolds hypersonic flow.

6 Conclusions

The drag coefficients for cones with hot and cold walls and different bluntness ratios have been found experimentally. There is a small wall temperature effect which can be accounted for by the change in the pressure drag that occurs in the free molecular limiting flow. The results from the Monte-Carlo calculations agree well with the experiments and they show that the flow field is characterised by the free molecular behaviour at least as far as $\mathrm{Kn}_{\infty,D} = 0.02$ and that the shear drag is the predominant force. From the experimental results it seems reasonable to conclude that the flow fields are characterised by the free molecular behaviour down to the lowest value of Knudsen number tested, equal to 0.006.

The nose bluntness effect on the measured drag can be correlated by normalising the coefficient by the value in the free molecular limit and by defining a Knudsen number based on the cone length.

Acknowledgement

The authors wish to acknowledge the support received for this research from the Science and Engineering Research Council and the Ministry of Defence.

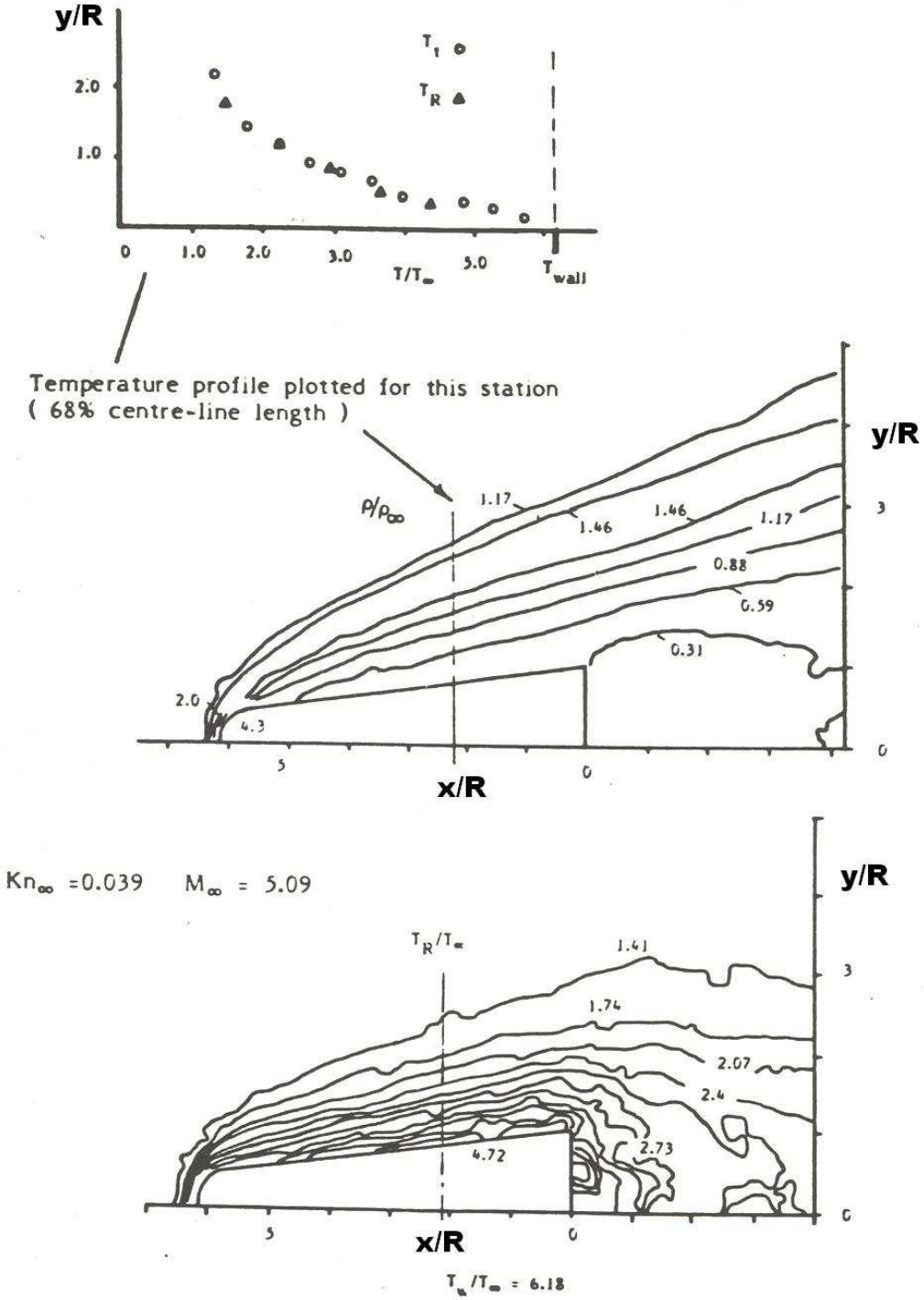

Figure 10: Computed density and rotational temperature for $T_w/T_0 = 1.0$. $\mathrm{Kn}_{\infty,D} = 0.039$, $\mathrm{M}_\infty = 5.09$. Fig. 10a as published.

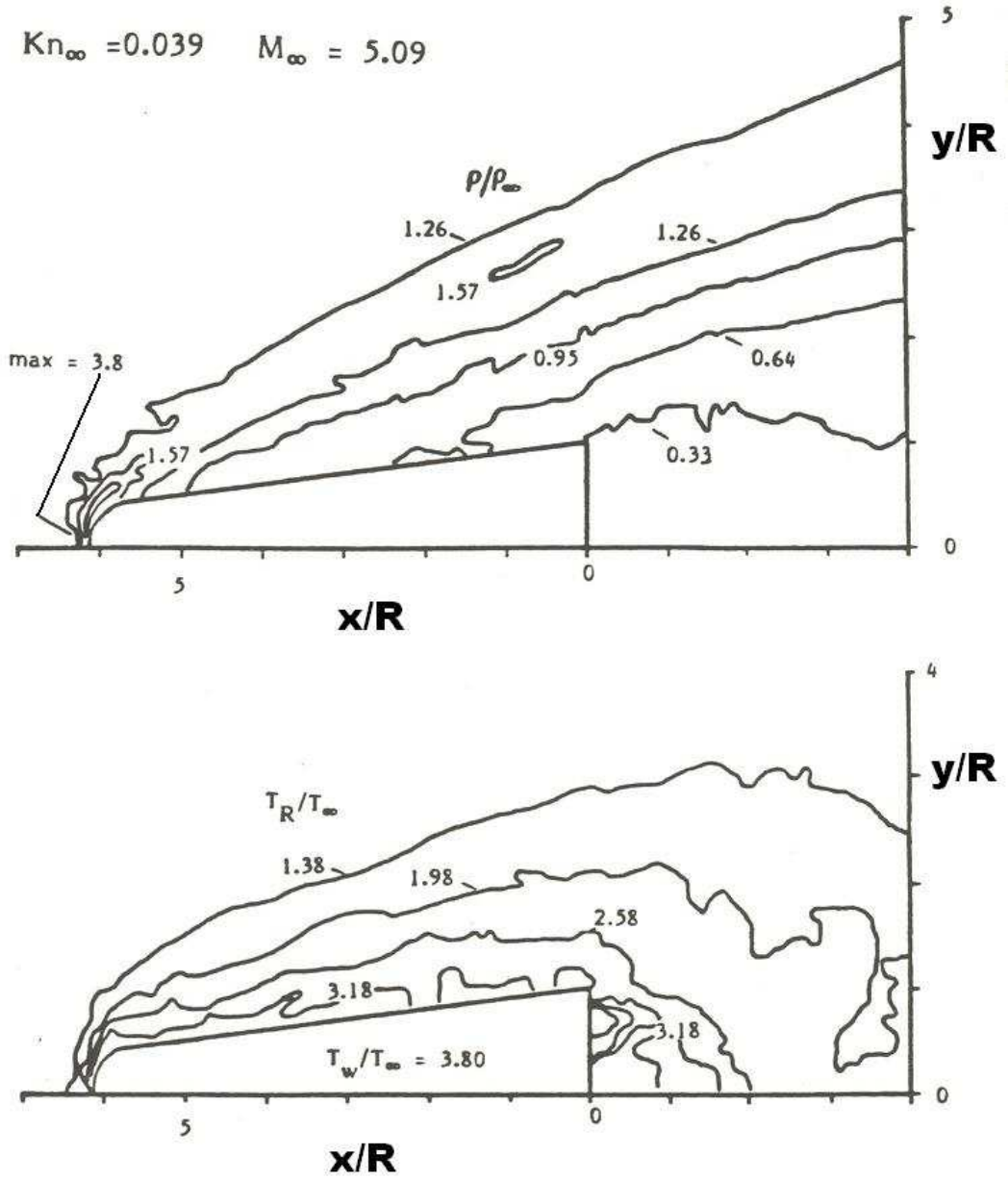

Figure 11: Computed density and rotational temperature for $T_w/T_0 = 0.61$. $\mathrm{Kn}_{\infty,D} = 0.039$, $\mathrm{M}_\infty = 5.09$. Figure 10b as published

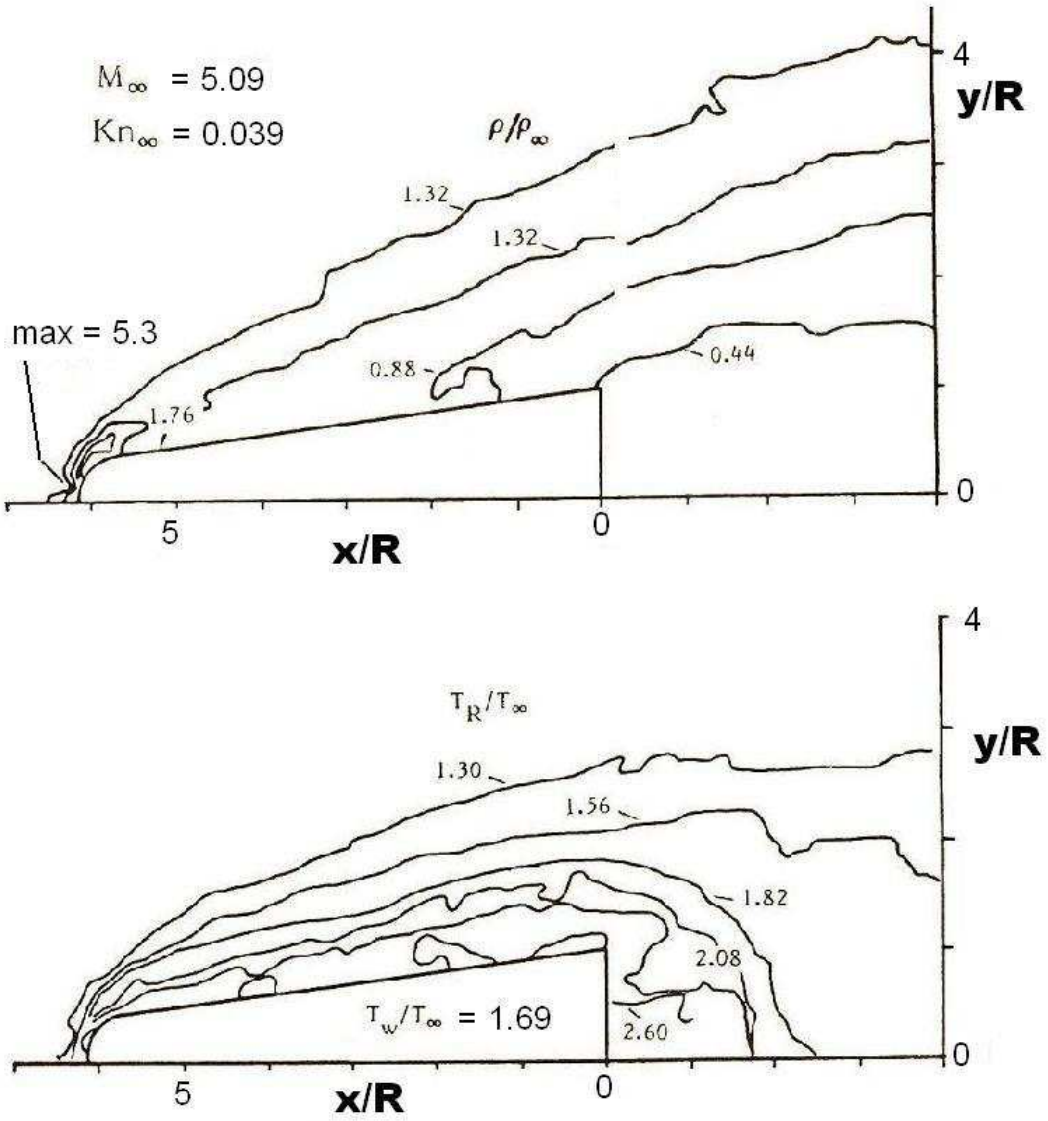

Figure 12: Computed density and rotational temperature for $T_w/T_0 = 0.27$. $\mathrm{Kn}_{\infty,D} = 0.039$, $\mathrm{M}_\infty = 5.09$. Figure 10c as published.

References

[1] Haslam-Jones, T. F. 'Measurements of the drag of slender cones in hypersonic flow at low Reynolds numbers using a magnetic suspension and balance', Oxford University Department of Engineering Science Report 1235/78, (1978).

[2] Dahlen, G. A. and C. L. Brundin 'Wall temperature effects on rarefied hypersonic cone drag', *Rarefied Gas Dynamics, 13th Symposium*, Novosibirsk, USSR, (*ed.* Rebrov).

[3] Hirschfelder, J. O., C. F. Cutiss and R. B. Bird *Molecular theory of gases and liquids* (2^{nd} ed), John Wiley and Sons, New York (1965).

[4] Davis, J., R. G. Dominy, M. N. Macrossan and J. K. Harvey 'An evaluation of some collision models used for the Monte Carlo calculations of diatomic rarefied hypersonic flows', *J. Fluid Mechanics*, **135**, p 355 (1983).

[5] Larsen, P. 1. and C. Borgnakke 'Statistical collision model for simulating polyatomic gas with restricted energy exchange' *Rarefied Gas Dynamics, 9^{th} Symposium* (ed. Becker and Fiebig), paper A7, DFVLR Press (1974).

— — —

Author's copy of: G. A. Dahlen, M. N. Macrossan, C. L. Brundin and J. K. Harvey, 'Blunt cones in rarefied hypersonic flow: experiments and Monte-Carlo simulations', *Proceedings of the 14^{th} International Symposium on Rarefied Gas Dynamics*, ed. H. Oguchi. University of Tokyo Press (1984), vol. I, pp. 229-240. ISBN 4-13-068109-5 (UTP 69092)